Progress in Organic Coatings 187 (2024) 108156

Contents lists available at ScienceDirect

Progress in Organic Coatings

journal homepage: www.elsevier.com/locate/porgcoat

# Implementing miniemulsion photopolymerization for synthesis of waterborne biobased poly(thioethers) coatings

Justine Elgoyhen [a], Cuong Minh Quoc Le [b,f], Alexander Ricke [c], Robert Liska [c], Stefan Baudis [c,d], Abraham Chemtob [b,f,**], Radmila Tomovska [a,e,*]

[a] POLYMAT and Department of Applied Chemistry, Faculty of Chemistry, University of the Basque Country UPV/EHU, Avda Tolosa 72, 20018 Donostia-San Sebastián, Spain
[b] Université de Haute-Alsace, CNRS, IS2M UMR7361, F-68100 Mulhouse, France
[c] Institute of Applied Synthetic Chemistry, TU Wien, Getreidemarkt 9/163 MC, 1060 Vienna, Austria
[d] Christian Doppler Laboratory for Advanced Polymers for Biomaterials and 3D Printing, Getreidemarkt 9, 1060 Vienna, Austria
[e] IKERBASQUE, Basque Foundation for Science, Plaza Euskadi 5, 48009, Bilbao, Spain
[f] Université de Strasbourg, 67034 Strasbourg Cedex 2, France

ARTICLE INFO

*Keywords:*
Bio-based thiol and ene
Miniemulsion polymerization
Waterborne polymer coatings

ABSTRACT

Herein, miniemulsion photopolymerization is implemented as a useful tool for synthesis of waterborne poly (thioether) dispersions from biobased monomers isosorbide-based dithiol (3R,3aR,6S,6aR)-hexahydrofuro[3,2-*b*] furan-3,6-diyl bis(3-mercaptopropanoate) and diallyl (3R,3aR,6S,6aR)-3,6-bis(allyloxy)hexahydrofuro[3,2-*b*] furan and their combination with the petroleum-based dienes diallyl terephthalate, 3,9-divinyl-2,4,8,10-tetraoxaspiro [5.5]undecane, and 1,4-bis(allyloxy)benzene. The synthetic process is optimized to achieve 30 % solids content latexes with weight average molecular weight ranging from 8.2 kg/mol to 136 kg/mol. The resulting poly(thioether) latexes yield consistent continuous polymer films after water evaporation at atmospheric conditions. Poly(thioether) films based on both biobased thiol and ene are soft and sticky, and thus, present insufficient mechanical properties for coating application. On the other hand, when biobased thiol was combined with petroleum based enes with aromatic and cyclic moieties within the structure, the obtained films are rigid and film forming. Only the film based on diallyl terephthalate diene present excellent balance of stiffness and flexibility, therefore with potential for coating application. Moreover, this film shows relatively good water sensitivity, with water uptake below 20 % after 11 days of water immersion and high gloss (above 80 gloss unit) measured at 60° angle of incidence. The properties are within the range of requirements for decorative coatings applications.

## 1. Introduction

"Biobased polymers" are produced, wholly or partly, with monomers directly extracted or derived from biomass, i.e. in this latter case, after one or several chemical modification steps [1]. A large majority of these so-called "biobased monomers" are reacted by step-growth polymerizations in homogeneous conditions, either in bulk or in solution [2]. By contrast, biobased monomers are less susceptible to chain (radical) polymerization either because they lack the required carbon-carbon double bonds, or when these latter are present, they are generally sluggish towards this type of polymerization [3]. Another challenge is that many biobased building blocks, such as fatty acids, terpene or phenol derivatives, are also prone to chain transfer reactions when they are chain polymerized, with the consequence of decreasing monomer conversion and polymer molecular weight [4].

However, chain radical polymerization is currently the mainstream mechanism for producing polymers in the form of particles aqueous dispersions, produced by polymerizations in dispersed media [5]. Thus, the production of high-molecular weight biobased polymer dispersions is limited because of the difficulty in finding suitable biobased monomers for chain radical polymerization, as most of the bio-molecules have to be functionalized with (meth)acrylic moieties prior to polymerization

* Correspondence to: R. Tomovska, POLYMAT and Department of Applied Chemistry, Faculty of Chemistry, University of the Basque Country UPV/EHU, Avda Tolosa 72, 20018 Donostia-San Sebastián, Spain.
** Correspondence to: A. Chemtob, Université de Haute-Alsace, CNRS, IS2M UMR7361, F-68100 Mulhouse, France.
*E-mail addresses:* chemtob@uha.fr (A. Chemtob), radmila.tomovska@ehu.eus (R. Tomovska).

https://doi.org/10.1016/j.porgcoat.2023.108156
Received 11 October 2023; Received in revised form 13 December 2023; Accepted 14 December 2023
Available online 27 December 2023

[6–8]. Although polymerizations in dispersed systems are already considered as eco-efficient due to the absence of volatile organic compounds and formation of waterborne products, the incorporation of biobased raw materials represents an opportunity to make them more sustainable and eco-friendly [9]. Specific biobased monomers able to react by chain polymerization in dispersed media were recently reviewed by Molina-Gutierrez et al. [6] More recently, a broader account of the subject was recently given by Aguirre et al. by including other biobased raw materials (surfactant, chain transfer agents, etc.) that make up waterborne polymer dispersions [10]. In only a few cases, biobased films formation and properties were investigated although coatings and adhesives are among the most important applications of polymer dispersions [11]. In most cases, fillers were added to the dispersions for mechanical reinforcement of the biobased polymer [12–14].

In this study, the possibility to carry out step-growth polymerizations in dispersed systems to yield biobased polymer dispersions for coatings has been revisited. Generally, the feasibility of step polymerizations in dispersed systems is severely decreased in presence of water, resulting in low molecular weight products and low functional groups conversion [15]. Interestingly, the radical-mediated polymerization of thiols with alkene monomers stands out as an exception since high molecular weight poly(thioether) dispersions have been recently achieved by emulsion and miniemulsion thiol-ene polymerizations [16–18]. Thus, one important question remains, whether similar heterogeneous step polymerizations could be performed with biobased thiol and ene monomers. There are precedents where bicomponent dithiol-diene monomer miniemulsions were polymerized. Between 2017 and 2019, the team of Araùjo used this process to polymerize petroleum-based dithiols with various biobased α,ω-diene monomers derived from castor oil-derived 10-undecanoic acid and 10-undecenoic acid [19,20]. In these previous studies, an application in the field of controlled drug delivery was targeted, and consequently, emphasis was made on particles' biocompatibility, cytotoxicity, degradability and cellular uptake. By contrast, monomer reactivity, polymer molecular weight, film-forming properties after water evaporation, film mechanical and thermal properties have been poorly investigated.

In this work, isosorbide-based dithiol (**Iso-SH**) and diallyl (**Iso-A**) biobased monomers were implemented in bulk or miniemulsion thiol-ene photopolymerization. Isosorbide is a starch-based biodegradable material and is thus considered one of the most promising plant-based platform chemicals [21].

The highly biobased bicomponent system **Iso-SH**/**Iso-A** was studied, but also three other formulations in which **Iso-SH** was polymerized with three petroleum-based dienes: diallyl terephthalate (**DATP**), 3,9-divinyl-2,4,8,10-tetraoxaspiro [5.5]undecane (**SPAC**), and 1,4-bis(allyloxy)benzene (**DAOB**). The molecular structures of the monomers are shown in Scheme 1.

In order to assess the polymerization behaviour, photopolymerization of these four thiol-ene mixtures was firstly conducted in a solvent-free condition. Double bond conversion, molecular weight, and moduli were determined using two main techniques: photorheology combined with real-time Fourier-transform infrared spectroscopy (RT-FTIR) and gel permeation chromatography (GPC). The same systems were then subjected to a miniemulsion photopolymerization. In this process, particle nucleation proceeds by radical entry into monomer droplets, subsequently converted into polymer particles [22,23]. Such droplet nucleation mechanism is suitable to the relatively water-insoluble monomers used in our study. By contrast, emulsion polymerizations involves a monomer diffusion process through the aqueous continuous phase, from the monomer droplets to the nucleated polymer particles, which is likely to be slowed down or prevented with poorly water-soluble monomers [6]. Herein, we aim at achieving colloidally stable polymer dispersions with solids content of 30 wt% and polymer chains with high weight average molecular weight ($M_w$ > 10 kg/mol) and film forming properties. The films exhibiting sufficient mechanical properties were subjected to a range of characterization by thermogravimetric analysis (TGA), differential scanning calorimetry (DSC), tensile and water uptake tests. Among the possible application of waterborne coatings and in regards of the obtained results, a special emphasis towards decorative coating was targeted and gloss tests were performed for that aim.

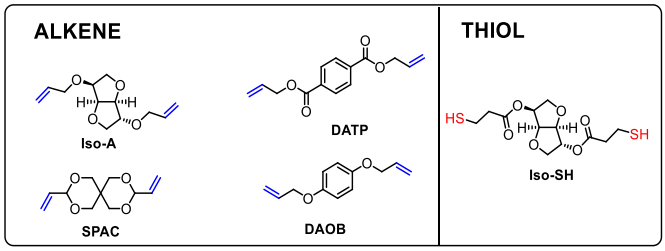


**Scheme 1.** Chemical structure of dithiol and diene monomers

## 2. Experimental

### 2.1. Material

All reagents were obtained commercially and used without further purification unless otherwise specified. The diene monomer diallyl terephtalate (DATP, 99.4 %), isosorbide (Iso, >98 %), allyl bromide (>98 %), 3-mercaptopropionic acid (>98 %), the photoinitiators lithium phenyl(2,4,6-trimethylbenzoyl)phosphinate (TPO-Li, >99 %) and diphenyl(2,4,6-trimethylbenzoyl) phosphine oxide (TPO, >98 %), paratoluenesulfonic acid (*p*-TsOH, >98 %), the radical inhibitors 2,5-di-tert-butylhydroquinone (DBHQ, >98 %) and hydroquinone (>99 %), and 3,9-divinyl-2,4,8,10-tetraoxaspiro[5.5]undecane (SPAC, >98 %) were purchased from TCI Chemicals. The photoinitiator 2,4,6-trimethylbenzoyldi-phenylphosphinate (TPO-L, >98 %) was supplied by Lambson (Satomer). Hexadecane (HD, 99.8 %) was purchased from Sigma. Tetrabutylammonium bromide (TBAB, >98 %) was purchased from AppliChem ITW Reagents. The surfactant alkyldiphenyloxide disulfonate (Dowfax 2A1, 45 %) was kindly provided by Dow chemicals. Commercial grade toluene, dichloromethane (DCM), petroleum ether (PE), and ethyl acetate (EE) were supplied by Donau Chemie. Commercial grade toluene (Donau Chemie) was dried using a PureSolv system (inert technology, Amesbury, MA). Commercial-grade acetone (Ac) was purchased from VWR and freshly distilled before usage.

### 2.2. Synthesis and purification of monomers

#### 2.2.1. Synthesis and purification of Iso-SH

In an oven-dried 1 L round-bottomed flask equipped with a Dean-Stark apparatus Iso (1 eq., 342.1 mmol, 50.0 g, Scheme 2), *p*-TsOH, (0.1 eq., 34.2 mmol, 6.5 g, Scheme 2) and 3-mercaptopropionic acid (2.5 eq., 855.3 mmol, 74.4 mL, Scheme 2) were solved in dry toluene (500 mL). The reaction mixture was stirred vigorously and heated to 130 °C in an oil bath overnight for 16 h. The reaction progress was monitored via thin layer chromatography (TLC) (PE:EE = 6:4, Rf (product) = 0.38, stain = potassium permanganate solution). The reaction was transferred into a separation funnel and subsequently washed four times by the addition of an aqueous $NaHCO_3$ solution (sat., 250 mL) and brine (2 × 150 mL). The organic phase was collected, dried over $NaSO_4$, and the solvent was evaporated under reduced pressure. The crude product was purified three times by column chromatography (PE:EE = 1:0 → 1:1) to yield the final product (3R,3aR,6S,6aR)-hexahydrofuro[3,2-*b*]furan-3,6-diyl bis(3-mercaptopropanoate) (**Iso-SH**, 78.3 g, 71 % yield, Schemes 1 and 2) as a colourless oil.

#### 2.2.2. Synthesis and purification of Iso-A

Iso (30.0 g, 1 equiv., 205.3 mmol, Scheme 3) was mixed with NaOH (18.1 g) and 50 mL of water. After complete solubilization of Iso, TBAB

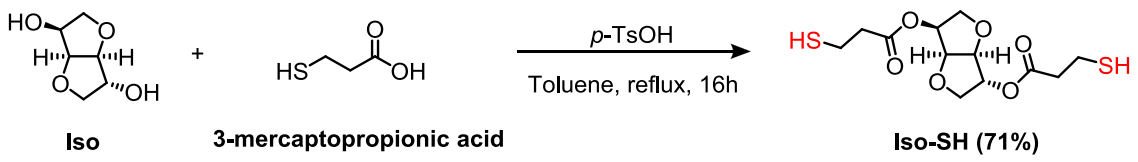


**Scheme 2.** Synthesis of Iso-SH

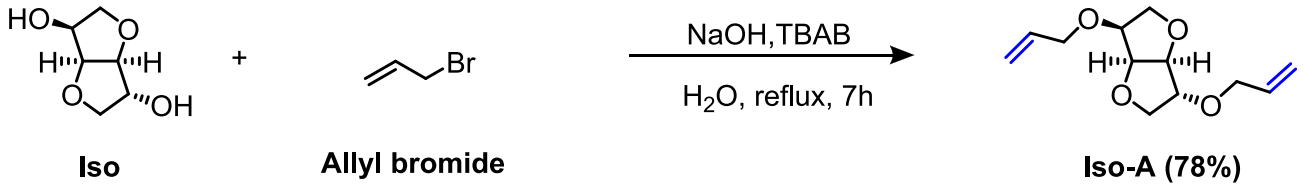


**Scheme 3.** Synthesis of Iso-A

(3.22 g) and allyl bromide (54.6 g, 451.6 mmol, Scheme 3) were added. This mixture was refluxed for 7 h. After cooling to room temperature, the aqueous solution was extracted with $CH_2Cl_2$ (4 × 50 mL). The organic phase was collected and washed with 1 M HCl (200 mL) and with deionized water (4 × 50 mL) to remove salts. Finally, the organic phase was dried over anhydrous $MgSO_4$, filtered, and $CH_2Cl_2$ was evaporated under vacuum. The crude product was purified two times via vacuum distillation (0.045 mbar, 95 °C), yielding the final product (3R,3aR,6S,6aR)-3,6-bis(allyloxy)hexahydrofuro[3,2-*b*]furan (**Iso-A**, 36.3 g, 78 % yield, Schemes 1 and 3) as a colourless oil.

Hydroquinone (18 g, 1 equiv., 163 mmol, Scheme 4) and potassium carbonate (31.6 g, 1.4 equiv., 229 mmol, Scheme 4) were dissolved in 200 mL dry acetone under inert atmosphere. The reaction mixture was heated to 45 °C and stirred for 10 min. Allyl bromide (31 mL, 360 mmol, 2.2 equiv., Scheme 4) was added. The reaction mixture was stirred and heated to 45 °C for 2 days. After filtration, the filtrate was concentrated and stored in the fridge for 10 min at −20 °C. White crystals formed. The crude product was recrystallized from hexane at −20 °C. The crystals were washed with 50 mL of hexane. The product was dried under vacuum over night to give 27.1 g of **DAOB** (87 % yield, Scheme 4) as white crystals.

*2.2.2.1. Column chromatography.* Column chromatography was performed with a Büchi Sepacore Flash System (Büchi pump module C-605, Büchi control unit C-620, Büchi UV-Photometer C-635, Büchi fraction collector C-660), using glass columns packed with silica gel 60 (0.040–0.063 mm; supplier: Merck) or aluminum oxide 90 neutral (pH (10 %) = 6.8–7.8; supplier: Carl Roth).

*2.2.2.2. Thin layer chromatography (TLC).* TLC was performed on aluminum TLC-plates coated with silica gel 60 $F_{245}$ (supplier: Merck) or neutral aluminum oxide 60 $F_{254}$ (supplier: Merck).

*2.2.2.3. Melting points.* Melting points were measured on an OptiMelt automated melting point system from SRS Stanford Research System. The heating rate was set to 0.5 °C $min^{-1}$.

*2.2.2.4. NMR.* NMR spectra were recorded on a Bruker Avance DRX-400 FT-NMR spectrometer at 400 MHz for $^1H$ and 100 MHz for $^{13}C$. The signals are reported with their chemical shifts δ in ppm and fine structure (s = singlet, d = doublet, t = triplet, q = quartet, qn = quintet, sep = septet, m = multiplet, br s = broad singlet). The chemical shifts were referenced using the respective NMR-solvent peak [$^1H$: $CDCl_3$ (δ = 7.26 ppm), $^{13}C$: $CDCl_3$ (δ = 77.2 ppm)] as an internal reference.

*2.2.2.5. High-performance liquid chromatography.* Monomers were also characterized by high-performance liquid chromatography (HPLC). HPLC measurements were conducted on a reversed-phase HP1100 Chemstation HPLC system equipped with a diode array and a Waters Xterra MS C18 column, 5 µm, 150·3.9 $mm^2$ inner diameter. Water/acetonitrile was used as a solvent system. Samples were prepared as 1 mg $mL^{-1}$ solutions in HPLC-grade acetonitrile.

### 2.3. Synthesis of biobased polymers by bulk photopolymerization

Bulk photopolymerization was performed by mixing thiol and ene in a stoichiometric ratio in presence of 1 wt% (based on monomers mass) of the photoinitiator TPO-L and subjected to RT-FTIR-photorheology measurements. For detailed information about the four formulations investigated, see Tables S1, S2, S3 and S4 supplied in Supporting Information.

#### 2.3.1. FTIR-RT-Photorheology

Measurements were performed on an *Anton Paar MCR 302 WESP*. A borosilicate glass plate with 60 mm diameter and 6 mm thickness and a PP25 stamp (25 mm diameter) were used. The rheometer was coupled with an FTIR spectrometer (*Bruker Vertex 80*) with external mirrors to guide the IR beam through the sample during the rheology measurements. After passing the glass plate, the IR beam is reflected at the PP25 measuring stamp and returns to the MCT-detector. More details about the setup can be found in literature [24]. All measurements were performed in triplicates at room temperature (20 °C). PE tape was glued to the borosilicate glass plate, and 180 µL sample volume was applied. The PE tape is necessary to remove cured samples after irradiation easily. A gap size of 200 µm between the measuring system (PP25) and the PE tape glued to the glass plate was set. For UV curing, an *Omnicure Series 200 EXFO* light source equipped with a broadband Hg-lamp (200 W) and a 400–500 nm filter was used. The light intensity was calibrated with an Ocean Optics USB 2000+ spectrometer at the surface of the PE Tape

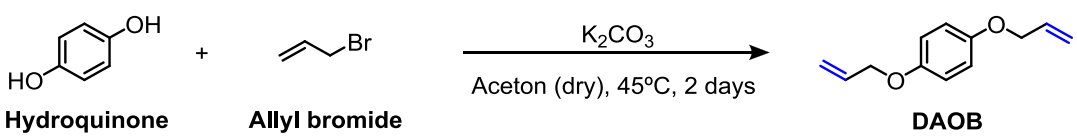


**Scheme 4.** Synthesis of DAOB

attached to the glass plate to 20 mW $cm^{-2}$. The samples were irradiated for 300 s. The photorheology measurements were analyzed with the software Rheoplus V3.62 from *Anton Paar*, and the IR spectra were analyzed with the software Opus 7.0 from *Bruker*. Due to the simultaneously measured NIR spectra, the double bond conversions (DBC) can be calculated using the area of the monitored absorption peak of the double bonds of allyl ethers at 6090–6175 $cm^{-1}$. The DBC is calculated from Eq. (1) for any time ($t$) of the polymerization process.

$$\text{Degree of Conversion} = \frac{A_o - A_t}{A_0} \times 100 \quad (1)$$

$A_0$ is the area of the absorption peak at time zero, and $A_t$ is the area of the absorption peak at the corresponding time of the photoinduced polymerization. The measurement data was then graphed and analyzed in Origin 2021b.

### 2.4. Synthesis of biobased polymers by miniemulsion photopolymerization

Table 1 summarizes all the monomer couples polymerized in dispersed media, the photoinitiator (PI) used for that aim and the irradiation conditions. In a typical reaction, an organic phase containing **Iso-SH** (3.4064 g, 10.57 mmol), **Iso-A** (2.3911 g, 10.57 mmol), the radical inhibitor DBHQ (0.0112 g, 10 mM with respect to monomer) and HD (0.36 g, 6.2 wt% with respect to monomer) was mixed in a 25 mL vial. The organic phase was then mixed with a 14 mL aqueous phase containing Dowfax 2A1 surfactant (0.18 g, 3.1 wt% with respect to monomer), and the photoinitiator TPO-Li (0.12 g, 0.40 mmol, 2.07 wt% with respect to monomer). A macroemulsion was then formed by high-speed mixing with Ultra-Turax setting at 15000 rpm for 5 min. The resulting macroemulsion was further emulsified by using a Branson sonifier SFX250 for 5 min at 90 % amplitude and pulse mode 5 s ON/1 s OFF cycles. The as-prepared monomer miniemulsion was irradiated for 60 min inside the custom-made photoreactor (3.7 mW $cm^{-2}$) with stirring speed at 1100 rpm.

Following similar procedure, polymer dispersions based on different combinations of **DATP**, **SPAC**, **DAOB** and **Iso-SH** monomers were prepared. Their preparation followed the same protocol as it was explained for the dispersion based on the monomers **Iso-A** and **Iso-SH**, with the reaction conditions, the PI used and irradiation parameters described in Table 1. In the Entry A1 from Table 1, the oil soluble photoinitiator TPO was used instead of TPO-Li. One miniemulsion was irradiated using a PESCHL photoreactor operating at an irradiance of 33 mW $cm^{-2}$ (385 nm) (Table 1, entry A3). The formulation of the polymer dispersion based on **DATP**, **SPAC**, **DAOB** and **Iso-SH** are addressed Tables S5, S6 and S7 in Supporting Information. Noteworthy, the reaction course does not provide controlled degree of polymerization/molecular weight, as well as copolymer composition for the synthesized polymers.

#### 2.4.1. Dynamic light scattering

The average particle size ($Z$-average diameter) and particle size distribution (PDI) of the miniemulsions and latexes were determined by dynamic light scattering (DLS) with a Vasco Particle size analyzer from Corduan technologies. The samples for analysis were prepared by dilution with Milli-Q water to solid content of 0.1 %, to avoid multiple light scattering. The Z-average diameter was taken from an average of 10 acquisitions in statistical mode with signal to noise threshold below 1 %.

**Table 1**
Poly(thioethers) synthesis conditions.

| Entry | Monomer | PI | Irradiance (mW $cm^{-2}$) |
|---|---|---|---|
| A1 | Iso-A/Iso-SH | TPO | 3.7 |
| A2 | Iso-A/Iso-SH | TPO-Li | 3.7 |
| A3 | Iso-A/Iso-SH | TPO-Li | 33 |
| B1 | DATP/Iso-SH | TPO-Li | 3.7 |
| C1 | SPAC/Iso-SH | TPO-Li | 3.7 |
| D1 | DAOB/Iso-SH | TPO-Li | 3.7 |

### 2.5. Poly(thioethers) characterization

#### 2.5.1. NMR

The chemical composition of the poly(thioethers) A3 (Iso-SH/Iso-A), B1 (Iso-SH/DATP), C1 (Iso-SH/SPAC) and D1 (Iso-SH/DAOB) was shown by $^1$H NMR. NMR spectra were recorded by means of a Varian 300 spectrometer (300 MHz). The spectra are supplied in Fig. S1, in Supporting Information.

#### 2.5.2. Gel permeation chromatography

Gel permeation chromatography (GPC) measurements, were performed on a Malvern VISCOTEK TDA system equipped with a ViscotekTDA 305-021 RI + Viscdetector, a UV Detector Module 2550 for TDA 305, and a VISCOTEK SEC-MALS 9 light scattering detector. Samples were prepared syringe-filtered (200 nm poly(tetrafluorethylene) syringe filters) 2–4 mg $mL^{-1}$ THF-solutions spiked with 0.5 mg $mL^{-1}$ butylated hydroxytoluene (BHT) as flow marker. GPC was conducted through PSS SDC column using dry THF as mobile phase at a flow rate of 0.8 mL $min^{-1}$ and a temperature of 35 °C. In the case of the triple detection, the dn/dc value was determined by injecting the sample at five different injection volumes between 80 and 120 µl and analyzing the slope of the signals. One narrow PS-standard ($M_w$ = 105 kg/mol) and one broad PS standard ($M_w$ = 245 kg/mol), both supplied by Malvern, were utilized for creating the triple detection calibration method. Analysis was conducted with the OmniSEC Software V5.12.461 (Malvern) to evaluate the elugrams and to calculate the number- and weight-average molecular weight ($M_n$ and $M_w$ respectively) and the dispersity $Đ$ of the polymers. In this work, the weight average molecular weight $M_w$ of the polymer are reported.

### 2.6. Films characterization

Self-supported films were prepared by casting the latex into silicon mold and dried at controlled temperature (25 °C) and humidity (55 %).

#### 2.6.1. Water uptake

Water uptake was measured by immersing films with similar shape and thickness in Milli-Q water in a close vial. The films were then withdrawn, gently dried with paper and weighted. The water uptake was determined as:

$$water\ uptake\ (\%) = \frac{m_t - m_0}{m_0} \times 100 \quad (2)$$

With $m_0$ weight of the film at $t_0$; $m_t$ weight of the film at time $t$.

#### 2.6.2. Thermogravimetric analysis

TGA of the films were carried out with a Perkin Helmer TGA 8000™ Thermogravimetric analyzer. Samples of 5–10 mg were heated from 40 °C to 800 °C at 10 °C $min^{-1}$.

#### 2.6.3. Differential scanning calorimetry

DSC experiments were carried out on Perkin Elmer DSC 8000 equipment from TA instrument using an Intracooler II as cooling system. Approximately 5 mg samples were encapsulated in sealed aluminum pans. For the non-isothermal procedure, the films based on **Iso-SH/Iso-A** and **Iso-SH/DATP** were heated up to 50 °C and the films based on **Iso-SH/DAOB** and **Iso-SH/SPAC** up to 100 °C at 20 °C $min^{-1}$, and kept 3 min in the melted state to erase thermal history. The sample was then cooled at 20 °C $min^{-1}$ until −30 °C for the films **Iso-SH/Iso-A** and **Iso-SH/DATP** and until −40 °C for the films **Iso-SH/DAOB** and **Iso-SH/SPAC**. Films were subsequently heated at 20 °C $min^{-1}$, up to 50 °C (films **Iso-SH/Iso-A** and **Iso-SH/DATP**). For the non-isothermal analysis of HD, the sample was heated until 60 °C at 20 °C $min^{-1}$, left 3 min in its melted state, and cooled at 20 °C $min^{-1}$ until 0 °C. Then, a final heating

ramp was performed at 20 °C $min^{-1}$ until 60 °C. For the non-isothermal procedure of films F.A1 and F.A2 samples were heated 30 °C above their melting point at 20 °C $min^{-1}$, up to 80 °C and left 3 min in the melted state. They were then cooled at either 1 °C $min^{-1}$ or 10 °C $min^{-1}$ until −30 °C and subsequently heated up at 20 °C $min^{-1}$ to 80 °C.

#### 2.6.4. Gloss measurement

The gloss of self-supported films was measured with a glossmeter from BYK Instrument at 20°, 60° and 85°.

#### 2.6.5. Tensile test

The mechanical properties of the films prepared for coatings applications were evaluated by tensile test. The measurements were carried out using the TA.HD plus texture analyzer (Stable Micro Systems Ltd., Godalmming UK). Flat "dog-bone" shaped tensile test specimens with dimensions of 15 mm 3.5 mm 0.5 mm were cut from dry films for the tensile test measurements. With a constant strain velocity of 1.5 mm $s^{-1}$ and a nominal strain rate of 0.1 Hz, stress-strain measurements were taken. Three specimens were prepared from each sample and the values presented are average of these measurements. The tensile properties for each material are represented in the stress-strain graphs.

#### 2.6.6. Atomic force microscopy

Morphological characterization of thin films was carried out by atomic force microscope (AFM), with a scanning probe atomic force microscope with a Dimension ICON atomic force microscope with a Nanoscope V controller (Bruker) operating in tapping mode. An integrated silicon tip/cantilever with a resonance frequency of around 300 kHz and a spring constant of 40 N/m was used, performing measurements at a scan rate of 1 Hz $s^{-1}$ with 512 scan lines. Different areas of each sample were analyzed to ensure the final morphology of the investigated films.

## 3. Results and discussion

### 3.1. Synthesis of biobased monomers

Biobased monomers **Iso-SH** (dithiol) and **Iso-A** (diene) were synthesized following reaction Schemes 2 and 3, respectively, and their synthesis was demonstrated by $^{1}$H NMR, $^{13}$C NMR. The signals are recorded according to their chemical shifts, which were reported in ppm (s = singlet, d = doublet, t = triplet, q = quartet, qn = quintet, sep = septet, m = multiplet, bs = brad singlet) in comparison to tetramethylsilane (d = 0 ppm). The spectra were then referenced on the used NMR-solvent [$^{1}$H: $CDCl_3$ (7.26 ppm), $^{13}$C: $CDCl_3$ (77.16 ppm)].

The signals recorded for the monomer **Iso-SH** are reported as follow: $^{1}$H NMR (400 MHz, Chloroform-*d*) *δ* 5.25–5.22 (m, 1H), 5.22–5.15 (dt, *J* = 5.9, 5.2 Hz, 1H), 4.87–4.82 (m, 1H), 4.51–4.47 (m, 1H), 4.00–3.91 (m, 3H), 3.86–3.79 (m, 1H), 2.82–2.63 (m, 8H), 1.74–1.68 (t, *J* = 8.2 Hz, 1H), 1.65–1.59 (t, *J* = 8.3 Hz, 1H). $^{13}$C NMR (100 MHz, Chloroform-*d*) *δ* 171.1, 170.8, 86.0, 80.8, 78.3, 74.3, 73.4, 70.6, 38.4, 19.8.

For the monomer **Iso-A**, signals are reported as follow: $^{1}$H NMR (400 MHz, Chloroform-*d*) *δ* 6.00–5.81 (m, 2H), 5.33–5.23 (m, 2H), 5.22–5.15 (m, 2H), 4.64–4.59 (m, 1H), 4.52–4.44 (m, 1H), 4.23–4.15 (m, 1H), 4.07–3.89 (m, 8H), 3.63–3.55 (m, 1H)·$^{13}$C NMR (101 MHz, Chloroform-*d*) *δ* 134.6, 134.3, 117.9, 117.6, 86.4, 83.9, 80.3, 79.6, 73.5, 71.7, 70.6, 69.9.

For the monomer **DAOB**, signals are reported as follow: $^{1}$H NMR (400 MHz, Chloroform-*d*) *δ* 6.85 (s, 4H), 6.12–5.97 (m, 2H), 5.40 (dt, *J* = 17.3, 1.6 Hz, 2H), 5.27 (dt, *J* = 10.5, 1.4 Hz, 2H), 4.49 (dt, *J* = 5.4, 1.5 Hz, 4H). $^{13}$C NMR (100 MHz, Chloroform-*d*) *δ* 153.0, 133.7, 117.6, 115.8, 69.6.

Melting point of **DAOB**: 36.2–38.1 °C.

Monomers were also characterized by HPLC. The monomer **Iso-SH** displayed a retention time of 3.18 min (20 % acetonitrile/(80 % water + 0.1 vol% trifluoroacetic acid), *v*/v, detection at 210 nm), and **Iso-A** of 2.54 min (20 % acetonitrile/(80 % water + 0.1 vol% trifluoroacetic acid), v/v, detection at 210 nm).

### 3.2. Synthesis of biobased polymers by bulk photopolymerization

Different types of thiol-ene polymers were synthesized, combining either both biobased monomers **Iso-SH** and **Iso-A**, or coupling the biobased thiol **Iso-SH** with oil-based diene monomers **DATP**, **SPAC**, and **DAOB**.

In order to examine the reactivity of the above-mentioned newly developed thiol-ene formulations and their properties as stiffness, flexibility, and crystallinity, a photorheology study was carried out in solvent-free conditions (bulk photopolymerization) by mixing stoichiometric amount of thiol and ene monomers in presence of the photoinitiator TPO-L. Through photorheology studies combined with real-time FTIR spectroscopy measurements, storage moduli (G′) of the thiol-ene polymers can be obtained, along to the corresponding final double bond conversion (DBCfinal) and the time until 95 % of the DBCfinal is achieved (t95%). This method links mechanical properties data of the bulk polymers with molecular information, and is particularly beneficial before heading to more complicated systems in dispersed media. The polymer samples obtained by the photorheology measurements were subsequently analyzed and characterized by GPC to determine polymers' $M_w$. The results of the RT-FTIR-photorheology measurements combined with the subsequent GPC analysis of the thiol-ene polymers obtained are depicted in Table 2.

In the case of the formulation based on **Iso-SH/Iso-A**, a high DBCfinal of 92 % was achieved as it would be expected in a pure step-growth reaction, and the time until 95 % of the DBCfinal is reached is comparable long (44 s). The polymer obtained presents very low storage modulus (G′final) of 13.8 kPa, in line with low $M_w$ of 6 kg/mol, typically observed for step-grown polymerization with conversion below 95 % [25]. These results highlight the flexibility and softness of the poly (thioether) based on this monomer pair, likely determined by the chemistry of the employed thiol-ene couple. Moreover, relatively low reactivity was observed in this system, which might be induced by a low efficiency of the primary radicals created from the photoinitiator to extract H from Iso-SH thiol. Nevertheless, as it might be seen in Table 2, Iso-SH thiol in combination with different enes initiated with the same TPO-L initiator polymerized much more efficiently, especially in case of **DAOB** and **DATP** enes. This fact indicates that the reactivity of thiol-ene click reaction is less efficient for this monomers' couple.

From these results, it is clear that the highly biobased latex based on **Iso-SH/Iso-A** monomer couple produced a very soft polymer, without sufficient mechanical strength for coating formulation. One of the strategies to strengthen the final polymer is to incorporate some aromatic ring [26] (with diallyl monomer such as **DAOB** or **DATP**) or spiro moieties [27] in the polymer building blocks. In addition, it is reported that thiol-ene polymer prepared with **SPAC** [27] can form semi-crystalline poly(thioether), and thus offering a way to improve mechanical property of its polymer film. This strategy was implemented here in order to strengthen the polymers. Even though the polymer is not completely bio-based, by replacing one part of the conventional oil-based polymers by bio-based one, the sustainability is already raised.

**Table 2**
Results of the RT-FTIR-photorheology measurements with the subsequent GPC analysis. The standard deviation for the final double bond conversion is lower than ±0.4 %. The standard deviation for the final storage modulus is always lower than ±0.01 MPa.

| Formulation | DBCfinal (%) | t95% (s) | $M_w$ (kg/mol) | $Đ$ | G′final (kPa) |
|---|---|---|---|---|---|
| Iso-SH/Iso-A | 92 | 44 ± 5 | 6.0 | 3.8 | 13.8 |
| Iso-SH/DATP | 99 | 17 ± 2 | 115.1 | 5.2 | 314.1 |
| Iso-SH/SPAC | 76 | 58 ± 7 | 9.1 | 3.6 | 617.3 |
| Iso-SH/DAOB | 98 | 14 ± 1 | 7.6 | 3.2 | 925.6 |

Additionally, once demonstrated the advantage of aromatic enes for strengthening of the thiol-enes, in future when more aromatic bio-based enes would be available, highly bio-based thiol-enes with sufficient performance for coating application can be produced.

When **Iso-SH** thiol was coupled with **DAOB**, **DATP**, or **SPAC** enes, again the type of ene affected the reaction rate and conversions achieved (Table 2). In particular, the DBCfinal of the thiol-ene couple **Iso-SH/DATP** is over 99 %, yielding to a very remarkable high $M_w$ of 115.1 kg/mol considering step-grown polymers. The reaction occurred rapidly, with 95 % of the final double bond conversion reached at 17 s, indicating very reactive monomers. The higher $M_w$ and the aromatic ring built within the polymer backbone gave rise to polymers with significantly higher G′final of 314.1 kPa. The formulation based on **Iso-SH** and **SPAC** is less reactive than its counterparts with low DBCfinal of 76 %, and 95 % of it was achieved relatively slow (after 58 s). Such low DBCfinal, along to poly(thioether) with relatively decent $M_w$ of 9.1 kg/mol are indication that the reaction is not only a pure step-growth reaction and that there is some homopolymerization of **SPAC** occurring. The polymer is even stiffer with G′final of 617.3 kPa. In case of **Iso-SH/DAOB**, presenting high conversion (98 %) and high reactivity, as the t95% is 14 s, the $M_w$ is surprisingly low (7.6 kg/mol), whereas the final storage modulus surprisingly high (925.6 kPa).

Despite that the photorheological study already present an idea about the polymerization reaction, reactivity and polymer properties, it was decided to continue the polymerization study in dispersed media for the four-monomer couples. Taking into consideration that the polymerization reactions performed in miniemulsion presents characteristic feature of radical compartmentalization within the small droplets/particles, the reaction rate can be enhanced due to decreased importance of bimolecular termination events, resulting in simultaneous rise in molecular weight, as it is the case for free radical emulsion polymerization of (meth)acrlyates [5].

### 3.3. Synthesis of biobased polymers by miniemulsion photopolymerization

As emphasized in the introduction, miniemulsion polymerization process has recently been shown to be particularly suited for the synthesis of polymers following a step growth mechanism, in which a stoichiometric ratio between monomers functionality is necessary to reach high conversion and molecular weights [18,26,28,29].

Herein HD is added to the formulation as a costabilizers and the surfactant Dowfax 2A1 is used to stabilize the miniemulsion against droplet coalescence. Dowfax 2A1, as well as HD, are non-reactive compounds and hence are not incorporated into the polymer chains, but they are incorporated into the polymer films and may affect the performance.

The main characterization of the synthesized poly(thioethers) latexes are reported Table 3, with the PI used, the *Z*-average diameter and PDI obtained from DLS and $M_w$ and $Đ$ obtained from GPC.

In the first system studied **Iso-SH/Iso-A**, 30 % solids content poly(thioether) dispersions (latexes) were obtained by photo-initiated miniemulsion polymerization (Entry A1-A3, Table 3 and Scheme 5a) and the synthetic process was optimized towards high molecular weight polymer chains. In a first attempt, the oil-soluble photoinitiator TPO was implemented to initiate the radical mediated step-growth polymerization, as it has been reported that when oil-soluble, it provides better particle size control than its water-soluble counterpart [18]. The oil-soluble photoinitiator, by forming radicals in the monomer droplets could indeed facilitate droplet nucleation and mitigate the contribution of the secondary nucleation process that induces formation of novel particles in aqueous phase. Secondary nucleation is usually undesired, because it widens the PDI and affects the polymer properties [5]. However, up to 43 % coagulation was obtained in the **Iso-SH/Iso-A** system after UV-exposure and the final particle size was of about 305 nm with relatively large PDI. Probably due to the UV light penetration depth and additional light scattering by the large droplets/particles, the interaction between TPO placed in droplets/particles and UV light was not efficient. In the conditions of lack of sufficient radicals flux, the nucleation process is likely slow, the colloidal stability is not on desired level, promoting coalescence of monomer droplets and particles aggregation. Therefore, low $M_w$ chains (8.2 kg/mol, entry A1, Table 3) were formed.

To avoid the mentioned challenges during synthesis, the oil-soluble PI was replaced by water soluble TPO-Li. Even though it gives rise to radicals in aqueous phase that start the polymerization with the few monomer units present in this phase, in the case of photopolymerization in dispersed media, likely there is a better light absorption resulting in efficient dissociation of the water soluble PI, giving rise to production of high radicals flux. It seems that this is a key issue to unlock the possibility of implementation of miniemulsion photopolymerization for thiol-ene synthesis. Subsequently, this reaction (entry A2, Table 3) yielded a coagulation-free polymer dispersion with higher polymer $M_w$ of 13.3 kg/mol, obtained for the same reaction conditions (irradiance 3.7 mW $cm^{-2}$ and 1 h of UV exposure). For the rest of the study, the water-soluble photoinitiator TPO-Li was hence preferred. No large difference in $M_w$ was observed when the irradiance was increased to 33 mW $cm^{-2}$ (Entry A3, Table 3), meaning that the denser photon flux did not affect the reaction and the polymer. Likely, the main factor limiting the $M_w$ in such conditions is the step-growth nature of the polymerization. It is worth mentioning that this behaviour is opposite than observed, when higher radical flux created under denser irradiation induced drop in the molecular weight of polyacrylates produced by chain-growth photoinduced miniemulsion polymerization [30]. The compartmentalization effect on the $M_w$ was shown to be similar as that in chain-growth polymerization system, and the $M_w$ were more than doubled in coagulation-free latex (entry A2). Nevertheless, we point out that in our experiments the irradiation conditions are different in the bulk and in miniemulsions, so it is difficult to be fully conclusive about the compartmentalization effect.

Even though decreasing the bio-based content, the previous bulk study demonstrated that the oil-based monomers containing aromatic ring or spiro moieties are promising in terms of material properties. This strategy was implemented by replacing the **Iso-A** monomer with **DATP**, **SPAC** or **DAOB** (Entries B1, C1 and D1, Table 3 and Scheme 5b, c and d) in the miniemulsion synthetic process. The idea here is to demonstrate that this strategy will work for the waterborne thiol-ene polymers produced from the bio-based thiol **Iso-SH**, which might be followed by eventual replacement of the oil-based enes used in this study by bio-based similar molecules, when available.

30 % solids content poly(thioether) aqueous dispersions were

**Table 3**
Poly(thioether) latexes, synthesis conditions and characterization.

| Entry | Monomer | PI | Irradiance (mW $cm^{-2}$) | % Coagulation | Z-average diameter (nm)/PDI | $M_w$ (kg/mol) | $Đ$ |
|---|---|---|---|---|---|---|---|
| A1 | Iso-SH/Iso-A | TPO | 3.7 | 43 | 305/0.24 | 8.20 | 2.32 |
| A2 | Iso-SH/Iso-A | TPO-Li | 3.7 | 0 | 285/0.20 | 13.3 | 2.31 |
| A3 | Iso-SH/Iso-A | TPO-Li | 33 | 0 | 308/0.19 | 15.86 | 2.75 |
| B1 | Iso-SH/DATP | TPO-Li | 3.7 | 0 | 168/0.06 | – | – |
| C1 | Iso-SH/SPAC | TPO-Li | 3.7 | 0 | 191/0.15 | 69.5 | 5.5 |
| D1 | Iso-SH/DAOB | TPO-Li | 3.7 | 0 | 141/0.16 | 136.4 | 7.8 |

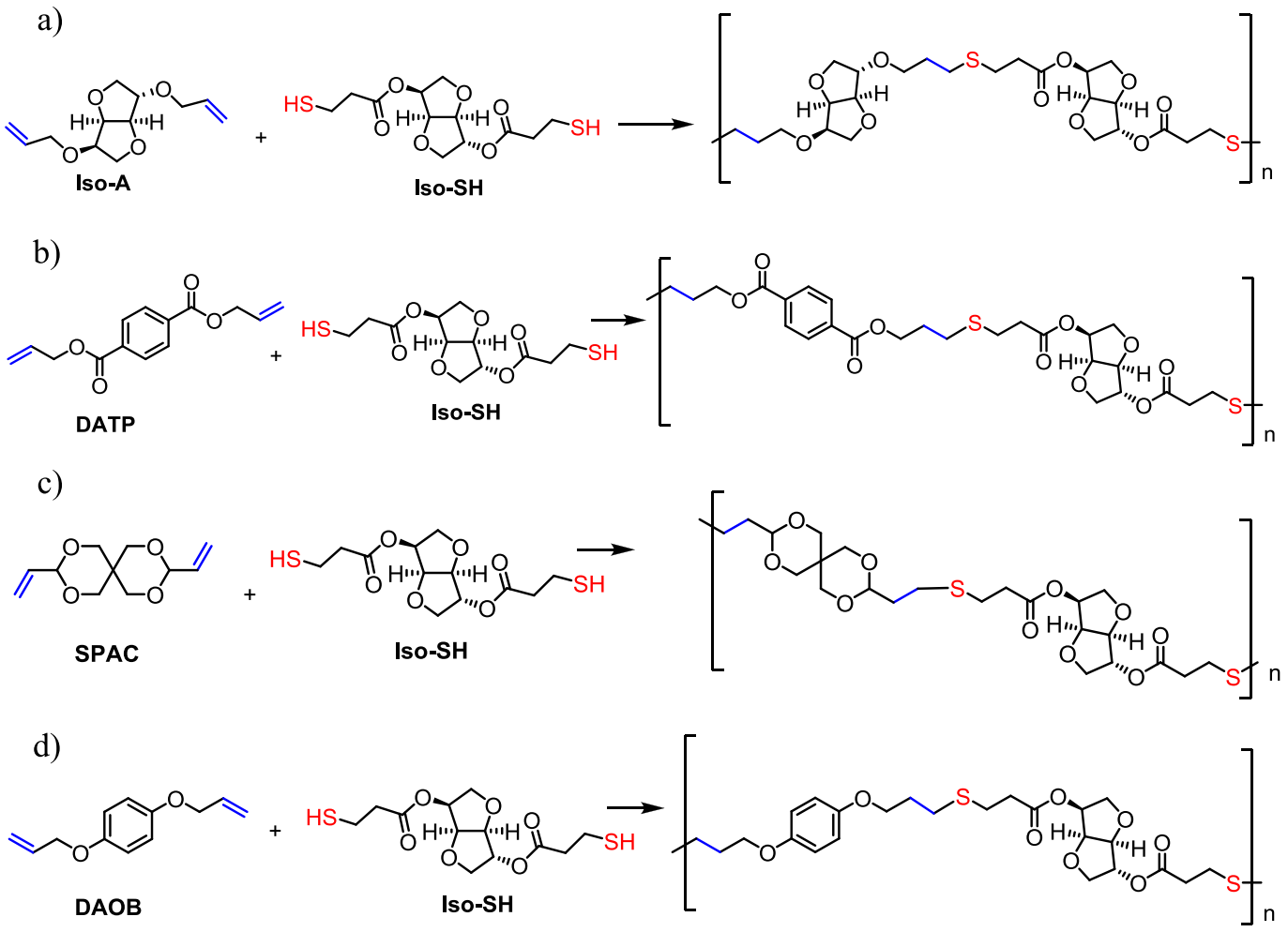


**Scheme 5.** Poly(thioether) obtained by photopolymerization in miniemulsion of the monomer pairs a) **Iso-SH/Iso-A** and b) **Iso-SH/DATP** c) **Iso-SH/SPAC** and d) **Iso-SH/DAOB**.

obtained by a photoinitiated polymerization in miniemulsion, performed under the selected conditions from the polymerization of monomer couple **Iso-SH/Iso-A** (TPO-Li initiator and 3.7 mW $cm^{-2}$). All dispersions produced were colloidally stable, with no coagulum formation. Similar particle sizes (below 200 nm) were obtained for the three dispersions, with narrow PDI, indicating fast droplet nucleation and lack of secondary nucleation processes. For the polymer based on **Iso-SH/DATP** couple, the polymer $M_w$ could not be determined by conventional GPC using THF or DMF, because the polymer was not soluble in neither of the two solvents. This may be due to high $M_w$ of the polymer chains or very high degree of crystallinity. As high degree of crystallinity is quite unlikely because of the complexity of the chemical structure that probably limits the rearrangement of polymer chains into crystal structure, we assume that the molecular mass should be very high. This is supported by the fact that much higher $M_w$ were obtained for the **Iso-SH/SPAC** and **Iso-SH/DAOB** polymers (Entry C1 and D1, 69.5 kg/mol and 136.4 kg/mol in Table 3, respectively) than the bio-based **Iso-SH/Iso-A** polymer. The $M_w$ achieved is 136.4 kg/mol, which is the highest obtained in this work and probably the highest reported for polymers obtained by step-growth polymerization. The higher $M_w$ of these semi-biobased polymers might be related to the small particle sizes in these cases, which are characterized with lower average number of radicals per particle and less bimolecular termination events, with respect to almost double particle size of the bio-based formulation **Iso-SH/Iso-A**.

The high $M_w$ combined with stiff yet flexible polymer chains could promote the formation of a coherent film. The four monomer couples, therefore might be polymerized in dispersed media, producing relatively concentrated polymer dispersions (30 %) with controlled particle size.

These results again show that much higher $M_w$ were obtained in miniemulsion than in bulk due to the mentioned radical compartmentalization effect within the small monomer droplets/particles. Moreover, it was observed previously in similar thiol-ene systems [31]. This phenomenon simultaneously provides fast polymerization rate and high molecular weights, because of the decrease significance of the bimolecular termination reactions, which moreover are predominant way of termination in step-growth mechanism.

### 3.4. Film formation and properties

In the scope of the aimed application in decorative coating, a continuous film has to be formed by water evaporation from cast polymer dispersions at standard atmospheric conditions ($T$ = 23 °C and relative humidity 55 %). Film formation is a complex process consisting of three main steps [32]. The first one involves evaporation of water and particles packing and ordering. In the following step, particles are deformed into a tetrahedral shape and the water is fully evaporated. At this stage, polymer particles retain their integrity and the film becomes optically clear as only one phase remains. The last step implies coalescence of the particles by polymer chains interdiffusion across particle-particle borders, which occurs at temperature above their glass transition temperature ($T_g$) and is driven by Brownian motion. Each step of the

film formation process can result in differences in the final film morphology and therefore will directly affect the final film properties. The last stage of the process is of primary importance when it comes to mechanical properties of the film. Indeed, good cohesion of a latex film is achieved when the polymer chains from different particles have interdiffused between them and created entanglements. For this, it is important that the $T_g$ of the polymer is slightly lower than the film forming temperature (lower than ambient temperature if the films should be formed at ambient conditions). On the other hand, too low $T_g$ may result in very soft polymer film that does not respond to the minimum requirements of mechanical resistance for coating application. These two contradictory requirements are the main challenge of the waterborne polymer films, which limits the possibility of improvement of their mechanical properties.

After water evaporation, the polymer dispersion based on the monomer couple **Iso-SH/Iso-A** gave rise to a soft and sticky film, as seen in the photos from Fig. S2 in the Supporting Information. Consistent, tough and glossy coating films were obtained from the dispersions based on **Iso-SH/DATP**, **Iso-SH/SPAC** and **Iso-SH/DAOB** in the same conditions (Figs. S2 b, c and d, Supporting Information), which is in accordance to the observation of storage modulus from bulk polymerizations. In addition, the films obtained are self-supported indicating a stiffness that can be attributed to the polymer structure (aromatic or cyclic structures) or/and to the presence of crystalline structures.

The production of continuous films at room temperature from the dispersions based on **Iso-SH/Iso-A**, **Iso-SH/DATP** and **Iso-SH/DAOB** suggests that the polymer chains efficiently interdiffused at this temperature and that the $T_g$ of these polymers are lower than 23 °C. In the case of the dispersion based on **Iso-SH/SPAC**, the appearance of cracks could indicate that the $T_g$ is higher than the temperature at which the film was produced. The $T_g$ of the films were measured by non-isothermal DSC analysis of the films (see DSC scans Fig. 1) and the values are listed in Table 4.

In the DSC scans Fig. 1, the exothermic peak appearing upon cooling is attributed to the crystallization of HD (occurring at around 10 °C), which subsequently melts in the heating scan around 20 °C as supported by the DSC scans Fig. S3 in Supporting information. The multimodal crystallization peaks and melting peaks in the DSC scans of the films in Fig. 1 indicate creation of different crystalline structures, either from HD or polymer chains, or other species present in the film such as the surfactant Dowfax 2A1, although they were not further investigated. As

**Table 4**
$T_g$ values for the films based on **Iso-SH/Iso-A**, **Iso-SH/DATP**, **Iso-SH/SPAC** and **Iso-SH/DAOB**. The values are depicted from the DSC heating scans in Fig. 1.

| Films | $T_g$ (°C) |
|---|---|
| Iso-SH/Iso-A | −2.3 |
| Iso-SH/DATP | * |
| Iso-SH/SPAC | 35.5 |
| Iso-SH/DAOB | 7.1 |

* The $T_g$ could not be observed in the range of temperatures employed for the analysis (between −30 °C and 50 °C).

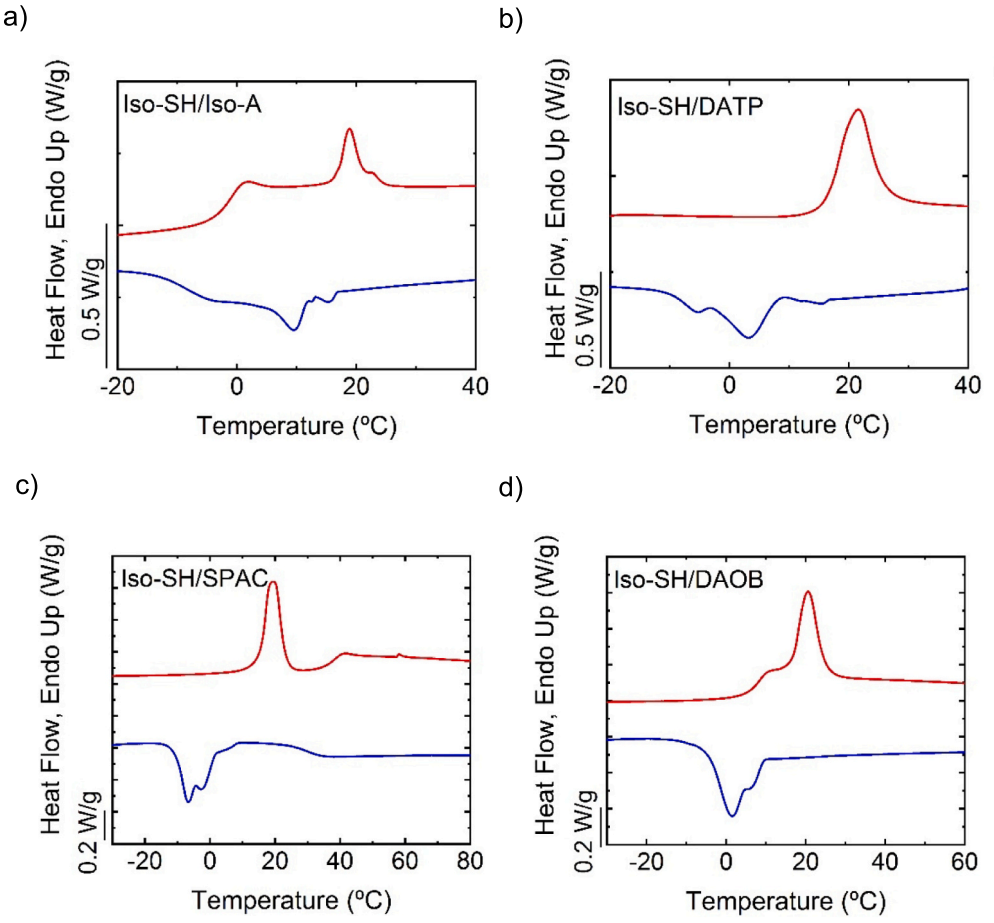


**Fig. 1.** DSC cooling scans from molten state at 20 °C $min^{-1}$ (blue) and subsequent heating scans at 20 °C $min^{-1}$ (red) for the films based on a) **Iso-SH/Iso-A**, b) **Iso-SH/DATP**, c) **Iso-SH/SPAC** and c) **Iso-SH-DAOB**. (For interpretation of the references to color in this figure legend, the reader is referred to the web version of this article.)

emphasized previously, however, polymer chains with such complex chemical structure (presence of aromatic and cyclic structures) are unlikely to organize into crystalline domains.

As expected, films based on **Iso-SH/Iso-A**, **Iso-SH/DATP** and **Iso-SH/DAOB** displays $T_g$ below room temperature, whereas the film based on Iso-SH/DAOB has a higher $T_g$ of 35.5 °C (Table 4), which is in line with the observations made previously.

Due to its flexibility and softness, the biobased film **Iso-SH/Iso-A** presents restrained utility as decorative coating film, but could find applications in other fields such as pressure sensitive adhesives (PSA), for example. The dispersions based on the monomer **pairs Iso-SH/SPAC** lead to brittle and rigid film (photo in Fig. S2c, Supporting Information), which prevented further characterization as the typical flat "dog-bone" shaped tensile test specimens to measure mechanical properties by tensile test cannot be prepared. Noteworthy, the film based on **Iso-SH/DAOB** (photo in Fig. S2d, Supporting Information), would display the best characteristic for coating application, with a high $T_g$, but still low enough to efficiently obtain film at room temperature. For the latter, unfortunately, further characterization in terms of mechanical properties are prevented because the film, probably too rigid, was too fragile.

In the following, attention was turned towards the film based on **Iso-SH/DATP** monomer couple that presents high potential for the aimed application. To elucidate the physical and mechanical properties of the film based on **Iso-SH/DATP**, further thermal analysis (TGA and DSC) and tensile tests were performed. The TGA thermogram of **Iso-SH/DATP** polymer is reported in Fig. 2a. In the investigated range of temperature, a first thermal decomposition occurred in a region of 100 °C and 200 °C and is attributed to the degradation of HD. To confirm it, TGA was performed on HD alone. HD thermogram is shown in Fig. 2b, confirming that it degrades between 100 °C and 200 °C.

The **Iso-SH/DATP** polymer film was thermally stable until 300 °C, as highlighted by the second thermal decomposition on the thermogram in Fig. 2a, which is in a range of waterborne (meth)acrylic polymers currently used for coating applications [33,34].

Mechanical resistance of the film **Iso-SH/DATP** was tested by tensile test measurements, as reported with the stress-strain plot in Fig. 3.

Fig. 3a shows that the **Iso-SH/DATP** film presents a relatively high Young's modulus of 3.72 MPa considering waterborne and step-grown polymers, and a high elongation at break of almost 55 %, highlighting the flexibility of the material. The tensile tests were performed at 23 °C, temperature at which the sample is completely amorphous as the melting peak of the crystalline structures observed by DSC is occurring at 21.5 °C. At lower temperatures, the presence of crystalline structures within the film could increase its stiffness and induce a drop in the elongation at break.

Water sensitivity of polymer films is an important characteristic of coatings. Water uptake measurements were performed on the **Iso-SH/DATP**-derived polymer in which the film specimen was immersed in water and evolution of the water absorption was monitored. The water uptake results are shown in Fig. 3b. The film **Iso-SH/DATP** presented relatively low water uptake after eleven days immersion in water of ~20 %, which is on the lower line of the water uptake rang of common (meth)acrylic or other hydrophobic coatings produced by emulsion polymerization [35].

Various parameters affect the water sensitivity of film coatings. The presence of ionic species in the polymer matrix increases the osmotic pressure, which is the major driving force of water uptake [32]. In the synthesis of the present polymers, few hydrophilic species that can contribute to the increased water solubility were used, such as TPO-Li water soluble initiator and Dowfax 2A1 surfactant. Indeed, hydrophilic moieties coming from the initiator are chemically incorporated within the polymer chains, increasing their hydrophilicity. In addition, the water sensitivity of the coating **Iso-SH/DATP** can be explained by the presence of inhomogeneities in the coating. As shown AFM images of the cross section of the films (Fig. 3c), the presence of pores in the biobased film **Iso-SH/DATP** could increase water penetration.

In the case of waterborne coatings, the migration of the water soluble surfactant has been reported to be an important drawback in water sensitivity [32]. Indeed, surfactants molecules provide hydrophilic channel that let the water soak in the coating. The surfactant Dowfax 2A1 is non-chemically bonded to the polymer, and its degree of compatibility with the polymer matrix affects its distribution within the film. However, the surfactant distribution is not static within the film. Free surfactant tends to migrate during and after the film formation process and affect the final properties of the film. If the chemical structures of the emulsifier and the polymer matrix are not compatible, emulsifier molecules aggregate within the polymer film matrix. These aggregates generate hydrophilic "pockets" able to absorb high water quantity from the surrounding. The reorganization of the surfactant depends on several factors, such as the hydrophobicity of the polymer matrix or its flexibility [32]. Highly hydrophobic polymers tend to be less compatible with amphiphilic surfactant, and flexible chains allow the surfactant to migrate readily. Hence, the supposedly low $T_g$ (that could not be measured by DSC in the range of temperature between −30 °C and 50 °C) and the hydrophobicity of the poly(thioether) based on **Iso-SH/DATP** tend to promote the reorganization of Dowfax 2A1 within the films into hydrophilic pockets, and therefore the water uptake of the film.

In the decorative coating aimed application, the visual appearance of the final film is very important. The visual appearance with respect to its gloss level can be measured with a gloss meter at different angles (20, 60 and 85°) and the results for the film **Iso-SH/DATP** are presented in Fig. 3d.

The coating **Iso-SH/DATP** presents high gloss, with a value higher than 80 at the angle 60° (Fig. 3d). Besides the aesthetic purpose, the differences between a gloss and matte effect affects the practical aspects of the coating such as surface cleanability or texture. Glossy surfaces show every imperfection, whereas matte surfaces tend to hide scratches

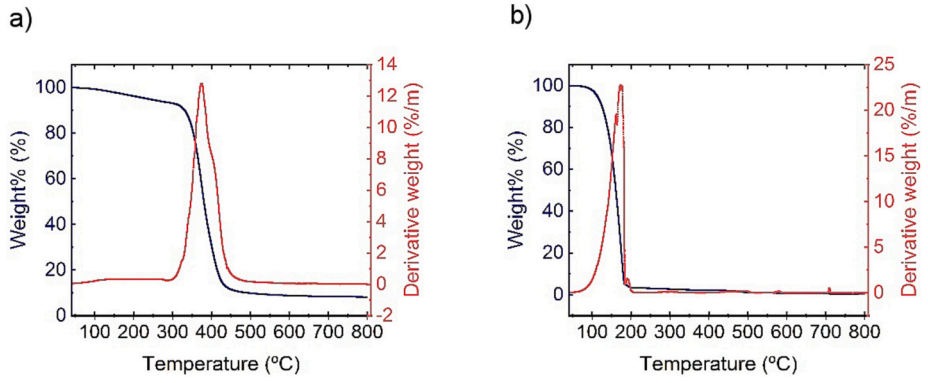


**Fig. 2.** TGA of a) the film based on the monomer pair **Iso-SH/DATP** and b) HD.

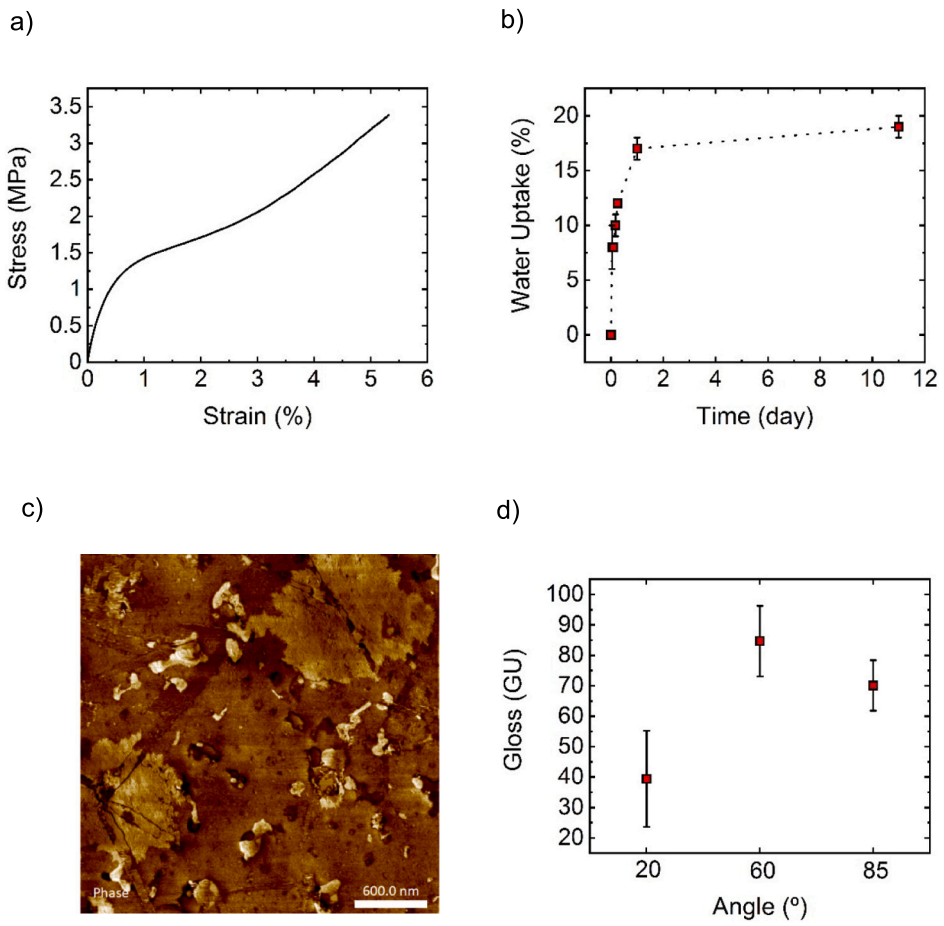


**Fig. 3.** a) Stress-strain plot from tensile test from the tensile measurements of the film **Iso-SH/DATP**, b) Water Uptake of the films **Iso-SH/DATP**, c) AFM images of the cross section of the **film Iso-SH/DATP** and d) Gloss measurement at 20, 60 and 85° angle for the film based on **Iso-SH/DATP**.

or imperfections. Moreover, the gloss can be an additional indication for migration of the surfactant to the film-air interface. For waterborne coatings, the higher the gloss, the less surfactant migrates to the film-air interface. Hence, in the case of the film Iso-SH/DATP, the surfactant may have mainly migrated within the coating forming the hydrophilic pockets, rather than at the film-air interface. This resulted in hydrophilic aggregates increasing water uptakes and causing the milky or cloudy appearance of the film. Indeed, the presence of water pockets due to water that was trapped within the coating during film formation, displays a lower refractive index and lead to the scattering of light.

## 4. Conclusion

In this work, we report implementation of miniemulsion photopolymerization for synthesis of 30 % solids content poly(thioethers) latexes, based on two newly synthesized biobased monomers **Iso-SH** and **Iso-A**. Namely, four thiol-ene monomer combination were implemented (**Iso-SH/Iso-A**, **Iso-SH/DATP**, **Iso-SH/DAOB** and **Iso-SH/SPAC**) and their step-growth polymerization in miniemulsion was studied, as well as their characteristics and possibilities for application as decorative coatings.

Noteworthy, the four polymer dispersions based on the biomonomers and their combination with oil-based monomers presented film forming abilities. Among them, the formulations containing biobased **Iso-SH** with the non-biobased dienes **DATP** could be further characterized for the aimed application in coating. Indeed, the film based on **Iso-SH/DATP** presented good thermal stability until 300 °C, and good mechanical properties, investigated by tensile test measurement, with a measured Young's modulus of 3.72 MPa and a 55 % elongation at break. In addition, the film **Iso-SH/DATP** presented relatively low water uptake after eleven days immersion in water of <20 %, induced on one hand due to amorphous structure in which very hydrophilic species are distributed (photoinitiator and surfactant), but as well due to the morphology that present small holes. In line with the aimed application in decorative coating, the film **Iso-SH/DATP** presents high gloss, with a value higher than 80 % at the angle 60 °C. Besides the aesthetic purpose, high gloss values provide another indication on the migration of the surfactant, which hence mainly migrates within the coating and not at the interface with air. Such behaviour is in line with the water uptake measurements.

Therefore, the synthesis in aqueous dispersed media, together with the incorporation of biobased building block within the polymer represents one step forward towards the production of highly biobased waterborne coating with added value.

## CRediT authorship contribution statement

**Justine Elgoyhen:** Writing – original draft, Visualization, Investigation, Formal analysis, Data curation. **Cuong Minh Quoc Le:** Investigation, Formal analysis, Data curation. **Alexander Ricke:** Investigation, Formal analysis, Data curation. **Robert Liska:** Supervision, Methodology, Conceptualization. **Stefan Baudis:** Supervision, Methodology, Conceptualization. **Abraham Chemtob:** Writing – review & editing, Supervision, Project administration, Methodology, Funding acquisition, Conceptualization. **Radmila Tomovska:** Writing – review & editing, Supervision, Resources, Project administration, Methodology, Funding acquisition, Conceptualization.

## Declaration of competing interest

The authors declare that they have no known competing financial interests or personal relationships that could have appeared to influence the work reported in this paper.

## Data availability

Data will be made available on request.

## Acknowledgements

The financial support of the European Union's Horizon 2020 research and innovation programme under the Marie Skłodowska-Curie grant agreement no. 765341 (project photo-emulsion, MSCA-ITN-2017) is gratefully acknowledged. We acknowledge funding from M-ERA.NET Network (project IMMENSE, IT-1525-22) and from the Basque Government through grant IT1503-22. Funding by the Christian Doppler Research Association within the framework of a Christian Doppler Laboratory for "Advanced Polymers for Biomaterials and 3D Printing" and the financial support by the Austrian Federal Ministry for Digital and Economic Affairs and the National foundation for Research, Technology and Development are gratefully acknowledged.

## Appendix A. Supplementary data

Supplementary data to this article can be found online at https://doi.org/10.1016/j.porgcoat.2023.108156.

## References

[1] R.M. Cywar, N.A. Rorrer, C.B. Hoyt, G.T. Beckham, E.Y.X. Chen, Bio-based polymers with performance-advantaged properties, Nat. Rev. Mater. 7 (2) (2022) 83–103, https://doi.org/10.1038/s41578-021-00363-3.
[2] S.L. Kristufek, K.T. Wacker, Y.Y.T. Tsao, L. Su, K.L. Wooley, Monomer design strategies to create natural product-based polymer materials, Nat. Prod. Rep. 34 (4) (2017) 433–459, https://doi.org/10.1039/c6np00112b.
[3] G. John, S. Nagarajan, P.K. Vemula, J.R. Silverman, C.K.S. Pillai, Natural monomers: a mine for functional and sustainable materials – occurrence, chemical modification and polymerization, Prog. Polym. Sci. 92 (2019) 158–209, https://doi.org/10.1016/j.progpolymsci.2019.02.008.
[4] W.S.J. Li, C. Negrell, V. Ladmiral, J. Lai-Kee-Him, P. Bron, P. Lacroix-Desmazes, C. Joly-Duhamel, S. Caillol, Cardanol-based polymer latex by radical aqueous miniemulsion polymerization, Polym. Chem. 9 (18) (2018) 2468–2477, https://doi.org/10.1039/c8py00167g.
[5] J.M. Asua, Emulsion polymerization: from fundamental mechanisms to process developments, J. Polym. Sci. Part A Polym. Chem. 42 (5) (2004) 1025–1041, https://doi.org/10.1002/pola.11096.
[6] S. Molina-Gutiérrez, V. Ladmiral, R. Bongiovanni, S. Caillol, P. Lacroix-Desmazes, Radical polymerization of biobased monomers in aqueous dispersed media, Green Chem. 21 (1) (2019) 36–53, https://doi.org/10.1039/c8gc02277a.
[7] K.K. Tremblay-Parrado, C. García-Astrain, L. Avérous, Click chemistry for the synthesis of biobased polymers and networks derived from vegetable oils, Green Chem. 23 (12) (2021) 4296–4327, https://doi.org/10.1039/d1gc00445j.
[8] E. Rigo, V. Ladmiral, S. Caillol, P. Lacroix-Desmazes, Recent advances in radical polymerization of bio-based monomers in aqueous dispersed media, RSC Sustain. 1 (4) (2023) 788–813, https://doi.org/10.1039/d3su00097d.
[9] F. Jasinski, P.B. Zetterlund, A.M. Braun, A. Chemtob, Photopolymerization in dispersed systems, Prog. Polym. Sci. 84 (2018) 47–88, https://doi.org/10.1016/j.progpolymsci.2018.06.006.
[10] M. Aguirre, S. Hamzehlou, E. González, J.R. Leiza, Renewable Feedstocks in Emulsion Polymerization: Coating and Adhesive Applications 1st ed., 56, Elsevier Inc., 2020 https://doi.org/10.1016/bs.ache.2020.07.004.
[11] S. Molina-Gutiérrez, W.S.J. Li, R. Perrin, V. Ladmiral, R. Bongiovanni, S. Caillol, P. Lacroix-Desmazes, Radical aqueous emulsion copolymerization of eugenol-derived monomers for adhesive applications, Biomacromolecules 21 (11) (2020) 4514–4521, https://doi.org/10.1021/acs.biomac.0c00461.
[12] P. Sarkar, A.K. Bhowmick, Terpene-based sustainable elastomers: vulcanization and reinforcement characteristics, Ind. Eng. Chem. Res. 57 (15) (2018) 5197–5206, https://doi.org/10.1021/acs.iecr.8b00163.
[13] D.H. Lamparelli, M.M. Kleybolte, M. Winnacker, C. Capacchione, Sustainable myrcene-based elastomers via a convenient anionic polymerization, Polymers (Basel) 13 (5) (2021) 838, https://doi.org/10.3390/polym13050838.
[14] Q. Xu, J. Ma, J. Zhou, Y. Wang, J. Zhang, Bio-based core-shell casein-based silica nano-composite latex by double-in situ polymerization: synthesis, characterization and mechanism, Chem. Eng. J. 228 (2013) 281–289, https://doi.org/10.1016/j.cej.2013.04.079.
[15] K.B. Mcauley, Step-growth polymerization, in: K.Y. Choi (Ed.), Polymer Reaction Engineering, Polymer Reaction Engineering, John Wiley & Sons, 2008, pp. 273–314, https://doi.org/10.1002/9780470692134.ch7.
[16] O.Z. Durham, D.V. Chapman, S. Krishnan, D.A. Shipp, Radical mediated thiol-ene emulsion polymerizations, Macromolecules 50 (3) (2017) 775–783, https://doi.org/10.1021/acs.macromol.6b02228.
[17] C.M. Quoc Le, M. Schmutz, A. Chemtob, Ab initio batch emulsion thiol–ene photopolymerization, Macromolecules 53 (7) (2020) 2369–2379, https://doi.org/10.1021/acs.macromol.0c00265.
[18] C.M. Quoc Le, L. Vidal, M. Schmutz, A. Chemtob, Droplet nucleation in miniemulsion thiol-ene step photopolymerization, Polym. Chem. 12 (14) (2021) 2084–2094, https://doi.org/10.1039/d1py00139f.
[19] T.O. Machado, P.B. Cardoso, P.E. Feuser, C. Sayer, P.H.H. Araújo, Thiol-ene miniemulsion polymerization of a biobased monomer for biomedical applications, Colloids Surf. B Biointerfaces 159 (2017) 509–517, https://doi.org/10.1016/j.colsurfb.2017.07.043.
[20] C.D.O. Romera, D. De Oliveira, P.H.H. De Araújo, C. Sayer, Biobased ester 2-(10-undecenoyloxy)ethyl methacrylate as an asymmetrical diene monomer in thiol-ene polymerization, Ind. Eng. Chem. Res. 58 (46) (2019) 21044–21055, https://doi.org/10.1021/acs.iecr.9b02386.
[21] D.J. Saxon, A.M. Luke, H. Sajjad, W.B. Tolman, T.M. Reineke, Next-generation polymers: isosorbide as a renewable alternative, Prog. Polym. Sci. 101 (2020), 101196, https://doi.org/10.1016/j.progpolymsci.2019.101196.
[22] F.J. Schork, Y. Luo, W. Smulders, J.P. Russum, A. Butté, K. Fontenot, Miniemulsion polymerization, Adv. Polym. Sci. 175 (2005) 129–255, https://doi.org/10.1007/b100115.
[23] J.M. Asua, Miniemulsion polymerization, Prog. Polym. Sci. 27 (7) (2002) 1283–1346, https://doi.org/10.1016/S0079-6700(02)00010-2.
[24] C. Gorsche, R. Harikrishna, S. Baudis, P. Knaack, B. Husar, J. Laeuger, H. Hoffmann, R. Liska, Real time-NIR/MIR-photorheology: a versatile tool for the in situ characterization of photopolymerization reactions, Anal. Chem. 89 (9) (2017) 4958–4968, https://doi.org/10.1021/acs.analchem.7b00272.
[25] G. Odian, Principles of Polymerization, 4th ed., Sons., J. W. &, 2004.
[26] F. Jasinski, A. Rannée, J. Schweitzer, D. Fischer, E. Lobry, C. Croutxé-Barghorn, M. Schmutz, D. Le Nouen, A. Criqui, A. Chemtob, Thiol-ene linear step-growth photopolymerization in miniemulsion: fast rates, redox-responsive particles, and semicrystalline films, Macromolecules 49 (4) (2016) 1143–1153, https://doi.org/10.1021/acs.macromol.5b02512.
[27] D.G. Sycks, D.L. Safranski, N.B. Reddy, E. Sun, K. Gall, Tough semicrystalline thiol-ene photopolymers incorporating spiroacetal alkenes, Macromolecules 50 (11) (2017) 4281–4291, https://doi.org/10.1021/acs.macromol.7b00628.
[28] E. Lobry, F. Jasinski, M. Penconi, A. Chemtob, C. Croutxé-Barghorn, E. Oliveros, A. M. Braun, A. Criqui, Continuous-flow synthesis of polymer nanoparticles in a microreactor via miniemulsion photopolymerization, RSC Adv. 4 (82) (2014) 43756–43759, https://doi.org/10.1039/c4ra06814a.
[29] F. Jasinski, E. Lobry, B. Tarablsi, A. Chemtob, C. Croutxé-Barghorn, D. Nouen, Le; Criqui, A., Light-mediated thiol-ene polymerization in miniemulsion: a fast route to semicrystalline polysul fide nanoparticles, ACS Macro Lett. 3 (9) (2014) 958–962, https://doi.org/10.1021/mz500458s.
[30] V. Daniloska, P. Carretero, R. Tomovska, J.M. Asua, High performance pressure sensitive adhesives by miniemulsion photopolymerization in a continuous tubular reactor, Polymer (Guildf). 55 (20) (2014) 5050–5056, https://doi.org/10.1016/j.polymer.2014.08.038.
[31] L. Infante Teixeira, K. Landfester, H. Thérien-Aubin, Nanoconfinement in miniemulsion increases reaction rates of thiol-ene photopolymerization and yields high molecular weight polymers, Polym. Chem. 13 (19) (2022) 2831–2841, https://doi.org/10.1039/d2py00350c.
[32] J.L. Keddie, A.F. Routh, Fundamentals of Latex Film Formation: Processes and Properties, Springer US, Berlin, 2010.
[33] K. Król-Morkisz, K. Pielichowska, Thermal Decomposition of Polymer Nanocomposites With Functionalized Nanoparticles, Elsevier Inc., 2018, https://doi.org/10.1016/B978-0-12-814064-2.00013-5.
[34] V. Kholodovych, W.J. Welsh, Thermal-oxidative stability and degradation of polymers, Phys. Prop. Polym. Handb. (1) (2007) 927–938, https://doi.org/10.1007/978-0-387-69002-5_54.
[35] F. Boscán, M. Meeuwisse, D. Mestach, M. Paulis, M.J. Barandiaran, S.J. Bohórquez, Incorporation of very insoluble monomers in waterborne coatings, Macromol. Mater. Eng. 304 (7) (2019) 1–9, https://doi.org/10.1002/mame.201900059.